Nanoscale

PAPER

View Article Online
View Journal | View Issue

Cite this: *Nanoscale*, 2023, **15**, 4932

Liquid-phase photo-induced covalent modification (PICM) of single-layer graphene by short-chain fatty acids†

Guilin Feng,[a] Tomoko Inose,[b] Nozomu Suzuki,[c] Han Wen,[a] Farsai Taemaitree,[a,d] Mathias Wolf,[e] Shuichi Toyouchi,[e,f,h] Yasuhiko Fujita,[g] Kenji Hirai *[a] and Hiroshi Uji-i*[a,b,e]

Received 30th November 2022,
Accepted 7th February 2023

DOI: 10.1039/d2nr06698j

rsc.li/nanoscale

We report an efficient photo-induced covalent modification (PICM) of graphene by short-chain fatty acids (SCFAs) with an alkyl chain at the liquid–solid interface for spatially resolved chemical functionalization of graphene. Light irradiation on monolayer graphene under an aqueous solution of the SCFAs with an alkyl chain efficiently introduces sp^3-hybridized defects, where the reaction rates of PICM are significantly higher than those in pure water. Raman and IR spectroscopy revealed that a high density of methyl, methoxy, and acetate groups is covalently attached to the graphene surface while it was partially oxidized by other oxygen-containing functional groups, such as OH and COOH. A greater downshift of the G-band in Raman spectra was observed upon the PICM with longer alkyl chains, suggesting that the charge doping effect can be controlled by the alkyl chain length of the SCFAs. The systematic research and exploration of covalent modification in SCFAs provide new insight and a potentially facile method for bandgap engineering of graphene.

Introduction

Graphene, a two-dimensional material consisting of a single atomic layer of sp^2 hybridized carbon, has attracted great attention as a next-generation material for opto-electronic devices, energy storage, catalysis, (bio-)chemical sensors, and so on since its isolation in 2004.[1–7] This is mainly due to its ultra-thin/light body along with its excellent mechanical strength/flexibility, high carrier mobility, unique optical properties, and high thermal conductivity.[8,9] However, the absence of a bandgap in graphene limits the advanced applications, especially in switching devices such as field-effect transistors.[10,11] To overcome this obstacle, several effective techniques to modify its electronic properties have been reported (known as bandgap engineering in graphene), for instance, by introducing sp^3-type defects in graphene. Unlike physical defects like vacancy, boundary, and edge defects, the sp^3-type defects can be reversibly introduced by electrochemical reactions, radical species, and electron or light irradiation.[12–14]

For practical applications, spatially resolved chemical modification remains challenging, although it is expected to be useful for site-specific control of wettability, catalytic or optical activity, molecular affinity, and electron conductivity.[15–18] Several methods for spatially resolved chemical modifications have been proposed, including masking, stamping, and light-induced ones.[1,19,20] Among these, photo-induced chemical modification (PICM) is a promising method. Liu *et al.* reported the photochemical reactivity of graphene in a toluene solution of benzoyl peroxide. They found that a Raman peak related to graphene defects (D-band) appeared only at the laser focus, where they suggested that photo-induced phenyl radicals attacked the basal plane of graphene forming covalent bonds.[21] Mitoma *et al.* found that excitation of graphene by visible light in the presence of water could result in graphene oxidation, which modifies the electronic transport properties,

[a]*Research Institute for Electronic Science (RIES) and Division of Information Science and Technology, Graduate School of Information Science and Technology, Hokkaido University, N20W10, Sapporo, Hokkaido 001-0020, Japan.*
E-mail: hirai@es.hokudai.ac.jp, hiroshi.ujii@es.hokudai.ac.jp
[b]*Institute for Integrated Cell-Material Science (WPI-iCeMS), Kyoto University, Yoshida, Sakyo-ku, Kyoto 606-8501, Japan*
[c]*Department of Human Studies, Faculty of Arts and Humanities, Shikoku Gakuin University, 3-2-1 Bunkyo-cho, Zentsuji, Kagawa 765-8505, Japan*
[d]*Institute of Multidisciplinary Research for Advanced Materials (IMRAM), Tohoku University, 2-1-1 Katahira, Aoba-Ward, Sendai 980-8577, Japan*
[e]*Department of Chemistry, Division of Molecular Imaging and Photonics, KU Leuven, Celestijnenlaan 200F, B-3001 Leuven, Belgium*
[f]*Department of Applied Chemistry, National Chiao Tung University, Hsinchu 30010, Taiwan*
[g]*Toray Research Center, Inc., Sonoyama 3-2-11, Otsu 520-8567, Shiga, Japan*
[h]*Research Institute for Light-induced Acceleration System (RILACS), Osaka Metropolitan University, Sakai, Osaka 599-8570, Japan*

† Electronic supplementary information (ESI) available. See DOI: https://doi.org/10.1039/d2nr06698j

suggesting local bandgap engineering.[22] We have extended this approach to deposit metal electrodes on the graphene upon visible laser light focusing on the interface between an aqueous solution of metal ions and the graphene surface.[23] We reported that multiple metal elements could be deposited on graphene in a site-specific manner just by changing the ion solution and revealed the excellent electric contact between the deposited metal and graphene. Besides the spatially resolved nature, PICM offers reversible graphene chemical patterning. Hirsch's group presented a strategy to functionalize graphene covered with dibenzoyl peroxide (DBPO) solid film by laser-direct writing with 532 nm and reading with 633 nm, followed by defunctionalization (erasing chemical patterns) by simple thermal annealing.[24] We recently reported an all-optical method for spatially resolved and reversible PICM of graphene in pure water using a one-color laser.[14] These reversible PICM offers a facile and flexible tool for site-specific control and tunability over the physicochemical properties of graphene.

Herein, we report that short-chain fatty acids (SCFAs) with an alkyl chain can offer an extraordinarily efficient PICM on graphene at the liquid phase. The PICM was performed in a site-specific manner by tightly focusing visible laser light (488 nm) on a graphene surface covered by an aqueous solution of the SCFAs. To investigate the alkyl chain length dependence on the PICM, HCOOH (Formic acid) and $CH_3(CH_2)_nCOOH$ (n = 0: acetic acid, n = 1: propionic acid, n = 2: butyric acid) were systematically investigated by means of Raman/IR spectroscopy. *In situ* Raman spectroscopy was carried out to record the change in the D-band intensity as a function of the irradiation time and the intensity ratio of the D- and G-bands (I_D/I_G) to evaluate defect formation in graphene. SCFAs with an alkyl chain (n = 0, 1, and 2) showed a higher reaction yield and rate than without alkyl chain (HCOOH), demonstrating that the alkyl chains ($(-CH_2)_nCH_3$) play a vital role in dense functionalization. The difference in the reaction rates and the shift of G-band peak position (G^-) between the SCFAs further confirms the roles of alkyl chains in introducing a high degree of charge doping effect on graphene. Raman and IR spectroscopy detected methyl, methoxy, and acetate groups at the modified area on graphene. This study proposes a plausible reaction mechanism for the liquid-phase PICM of graphene and paves a way to tune the charge doping effect for graphene bandgap engineering.

Experimental section

Sample preparation

The monolayer graphene on a polymer film was purchased from Graphenea. Graphene monolayers were deposited onto a clean coverslip. In short, monolayer graphene sandwiched between a polymer layer and a sacrificial layer was dipped into deionized water, where the polymer layer was detached and the graphene covered with the sacrificial layer floated on the water surface. A clean coverslip was dipped into the water at a leaned angle to fish out the monolayer graphene/sacrificial layer. The sample was dried in air for 30 min at room temperature and moved to the oven (Standard Electric Furnace, FO201, Yamato) to keep at 150 °C for 1 h and was stored under a vacuum environment for at least 24 h to firmly attach the graphene to the substrate. The sacrificial layer on graphene was removed by hot acetone (50 °C, 1 h) two times and isopropanol (1 h). Then the transferred sample was stored in a vacuum environment for at least 24 h prior to the experiment.

Chemicals

Milli Q water is obtained from a Milli-Q-plus system with a resistivity greater than 18 MΩ cm^{-1}. Formic acid, acetic acid, propionic acid, and butyric acid were purchased from Tokyo Chemical Industry Co., Ltd (TCI) and used without further purification.

Raman spectroscopy

Raman spectroscopy was carried out using an inverted optical microscope (Ti-U, Nikon) equipped with a piezoelectric sample stage. A continuous-wave 488 nm laser (Sapphire SF 488-100 CW CDRH) was used for the PICM of graphene. The laser was reflected and guided into an objective (PlanFluor, ×60, N.A. 0.95, Nikon) using a long-pass dichroic mirror (zt488rdcxt, Chroma®) for a 488 nm laser line. The laser power at the sample was ~6 MW cm^{-2} for photo-covalent functionalization, which was adjusted by attenuators with different optical densities. Raman scattering light from the sample was collected by the same objective and guided to the spectrograph (iHR320, Horiba, cooled to −75 °C) equipped with a 600 lines per mm grating. A long-pass filter (ET500LP for 488 nm line) and a pinhole (diameter 100 μm) are placed before the spectrograph entrance to reject Rayleigh scattering and out-of-focus contribution, respectively. All photo-covalent modification and Raman mapping were conducted by OMEGA software (CombiScope, AIST-NT/Horiba). OMEGA software (AIST-NT/HORIBA), Igor Pro, Origin Lab 9.1, and MATLAB (MathWorks) were used for Raman data analysis. Transmission/wide-field luminescence/wide-field Raman imaging was performed using a charge-coupled device (CCD) camera (ImagEM, Hamamatsu Photonics) operated at −65 °C, where a long-pass filter (ET500LP, Chroma) was inserted in front of the camera.

Density functional theory (DFT) calculations

Density functional theory (DFT) calculations were carried out to estimate the Raman peaks related to SCFA. Each structure was fully optimized by the DFT calculations using the B3LYP functional with the 6-31G(d) basis set in Gaussian 16 software (Gaussian, Inc., Pittsburgh, PA). The theoretical Raman spectrum was calculated for each energy-minimized structures at B3LYP/6-31G(d) level of theory by freezing the coordinate of the graphene moiety.[26]

IR spectroscopy

Graphene was transferred on a $ZnSe_2$ plate prior to the PICM for IR measurement. Monolayer graphene/$ZnSe_2$ was functionalized in aqueous solution of acetic acid (1 M) by irradiating

with visible light from a Xenon lamp. IR spectroscopy was conducted with Nicolet continuμm microscope (Thermo Fisher, Inc.) under transmission mode. The spectral range was set to 4000–650 cm^{-1} with 8 cm^{-1} resolution (Accumulation: 4096 times). The detection area was set to 100 × 100 μm^2. Spectrum processing was carried out with OMNIC and IGOR pro software.

Results and discussion

Fig. 1a illustrates a typical PICM configuration at a liquid–solid interface on graphene monolayers supported by a dielectric substrate. A laser line at 488 nm (laser power: 0.1–10 MW cm^{-2}) was tightly focused with an objective lens (NA ~0.95) on a graphene surface in the presence of water or an aqueous solution of the SCFAs. Raman spectra were simultaneously recorded using the same objective lens and a spectrograph equipped with a CCD, allowing *in situ* Raman monitoring during the PICM processes. To confirm the spatial distribution of the PICM, Raman mapping around the modified area is taken under weak laser power (0.1 MW cm^{-2}) to ensure that the Raman excitation light would not induce further PICM. Fig. 1b presents typical Raman spectra of a graphene monolayer before and after PICM under an aqueous solution of acetic acid at a laser power of 6 MW cm^{-2}. Before the PICM (0 s), only the G-band at 1595 cm^{-1} and 2D-band at 2697 cm^{-1} were observed, indicating pristine graphene, where the G-band is assigned to the graphitic E_{2g} mode from sp^2-hybridized carbon atoms and 2D-band to the double resonance scattering process between nonequivalent K points in the Brillouin zone of graphene.[25] In contrast, after the PICM, an additional peak around 1350 cm^{-1} appears, which can be assigned to the D-band (defect mode[27]). Since the D-band disappears after thermal treatment of the graphene at 350 °C in the air, as shown in Fig. S1,† it is mainly due to a chemical defect instead of a physical one in accordance with literature.[27] The same decrease of I_D/I_G in acetic and propionic acid solution suggests similar defects are introduced on graphene. The small difference in I_D/I_G ratio after heating (0.21 for acetic acid and 0.26 for propionic acid) could be attributed to the functional groups on graphene surface. Fig. 1c shows D-band intensity maps before and after PICM at a fixed point. Before high-power laser irradiation, the Raman intensity map does not show any features (Fig. 1c top left). After high-power laser irradiation, however, the Raman map shows a point with high D-band intensity (Fig. 1c top right). Since the laser focus was fixed precisely at this point during the PICM process, the map indicates that the PICM was induced only around the laser focal point. The full-width half-maxima (FWHM) of this point was estimated to be *ca.* 1.2 μm (Fig. 1c bottom), which is larger than the diffraction limit (~260 nm). This suggests that radicals or hot electrons generated upon light irradiation diffuse over the diffraction limit and react with the nearby graphene surface or surrounding molecules.[14,22]

In this study, we compare the PICM processes of graphene monolayers in pure water, formic acid (HCOOH), acetic acid, propionic acid, and butyric acid; $CH_3(CH_2)_nCOOH$ (n = 0, 1, and 2, respectively). Fig. 2 displays Raman spectra of graphene after the PICM for 120 s in an aqueous solution of each molecule. In all cases, D-band was confirmed after PICM. However, the intensity of the D-band in the case of the SCFAs with an alkyl chain is significantly higher than those of pure water and formic acid. The D to G ratio (I_D/I_G) reaches about 1 for the SCFAs with alkyl chain, while it remains below 0.5 for water and formic acid under the employed illumination condition. Another striking difference between them is the graphene Raman intensity after the PICM. The Raman peak intensities after PICM with the SCFAs with alkyl chain were significantly enhanced (typically reaches 10 000 counts per s) compared to those before the PICM (typically 2000 counts per s), while it remains the same in the case of water and formic acid. It is likely that graphene electronic structures are modified by the PICM with SCFAs with an alkyl chain.

To investigate the PICM dynamics, *in situ* Raman monitoring was conducted during the PICM process in water and an

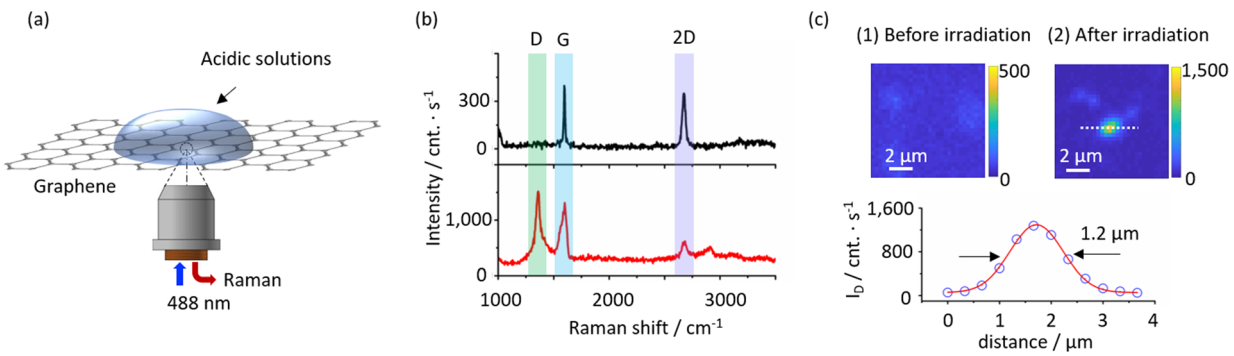

Fig. 1 Principle of PICM on graphene at the liquid solid interface. (a) A schematic illustration of *in situ* Raman spectroscopy during PICM. A 488 nm laser was used for both PCIM and Raman spectroscopy. (b) Typical Raman spectra of a graphene monolayer before (gray) and after (red) PICM for 0 and 120 s, respectively, at an interface between graphene and an aqueous solution of acetic acid. (c) Typical maps of the Raman intensity at 1350 cm^{-1} before and after PICM at a laser focal point (above) and a line profile along (open circle) the white dashed line in the map after irradiation with a Gaussian fitting (solid red line) (FWHM ~1.2 μm).

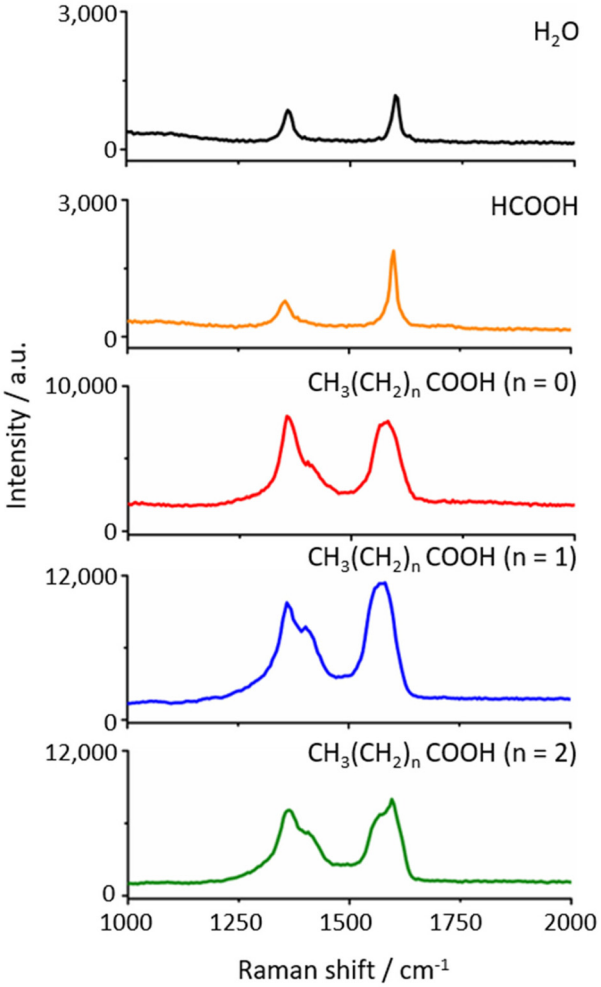

Fig. 2 Raman spectra of graphene after 120 s PICM in H_2O, formic acid, acetic acid (n = 0), propionic acid (n = 1), and butyric acid (n = 2), respectively, from the top to the bottom panels.

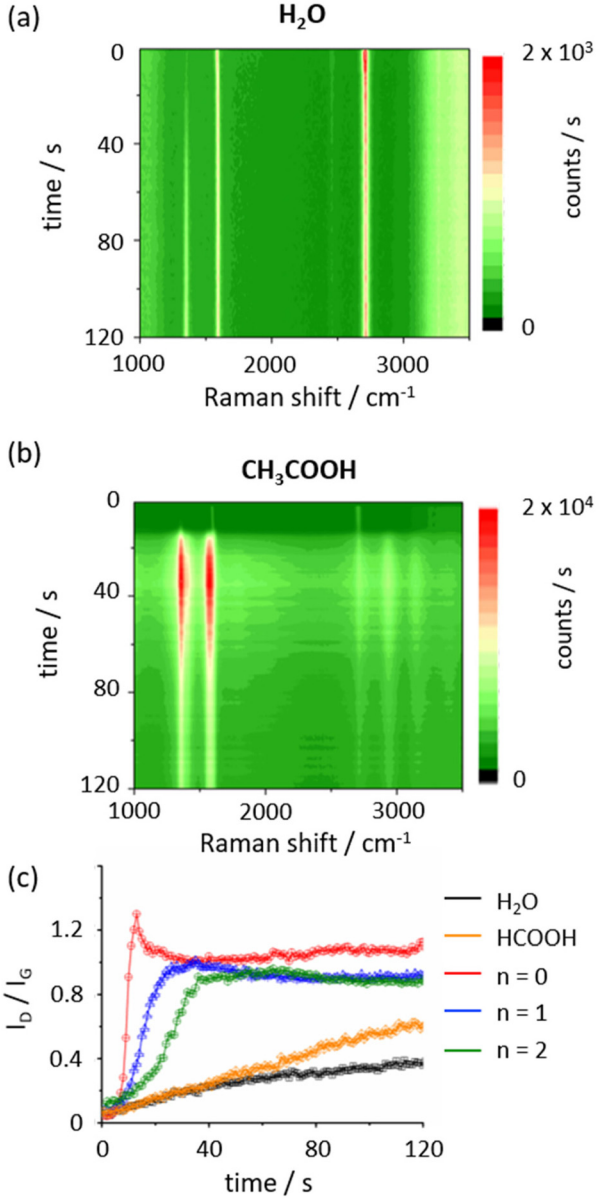

Fig. 3 Time-course of Raman spectroscopy during the PICM. Waterfall plot of Raman spectra of graphene modified in H_2O (a) and acetic acid (b), respectively. (c) The intensity ratio between D and G bands (I_D/I_G) as a function of time for the PICM in H_2O (black), formic acid (orange), acetic acid (n = 0) (red), propionic acid (n = 1) (blue), and butyric acid (n = 2) (green), respectively.

aqueous solution of acetic acid (0.1 M). Fig. 3a and b, respectively, present waterfall plots of the Raman scattering as a function of time during the PICM process in water and 0.1 M acetic acid aqueous solution (the plots in propionic and butyric acid are presented in Fig. S2†). The corresponding I_D/I_G ratios as a function of time for the solutions are summarized in Fig. 3c. $I_D/(I_D + I_G)$ ratios are also estimated and show almost the same trend as I_D/I_G (Fig. S3†), indicating a slight change of I_G at the initial state is negligible for kinetics analysis. Hereafter, the reaction is analysed based on the I_D/I_G. First, water and the formic acid solution show a similar trend, *i.e.*, I_D/I_G values gradually increase as a function of time. In contrast, the SCFAs with alkyl chain reveal completely different behaviour; at the first stage (0–10 s in the case of acetic acid), G- and D-bands show a similar trend as water and formic acid, while the intensity of both G- and D-bands suddenly increase by a factor of 5–6 (Fig. 3b and Fig. S2†). The maximum I_D/I_G values reach a plateau at ~1 within 20 s for acetic acid and at 0.8 within 40 s for propionic and butyric acid, while it takes a few minutes in the case of water and formic acid solution. These results imply that the PICM mechanism for SCFAs with an alkyl chain differs from that for water and formic acid solution. In addition, we observed I_D decreases after a period of PICM time and this suggests the more functional groups on graphene make larger changes of electronic structures of graphene, resulting in maximum of D peak intensity during PICM process at the certain excitation energy due to resonant Raman scattering.[28]

Since the I_D/I_G ratio is related to the reactions of graphene and follows an exponential fashion at the abrupt increase in

the initial part of the time course, the initial reaction rate constant can be estimated from the rise in I_D/I_G plot with the following equation,[22]

$$I_D/I_G\ (t)\ \propto\ \exp(kt) - 1 \qquad (1)$$

where the time constant k is defined as the rate of loss of sp^2 carbon atoms of graphene during PICM process. As summarized in Table 1, k values for SCFAs with an alkyl chain are 100 times higher than those of water and formic acid. The fitting details were presented in Fig. S4.† A successive decrease was found in the reaction rate with increasing alkyl chain length, suggesting the length of the alkyl chain affects the generated radical's activity.

In order to identify the chemical reactions of the PICM on graphene, detailed analyses with luminescence, IR, and Raman spectroscopy have been conducted. For the spectroscopic analyses, a wide area of monolayer graphene was periodically modified by laser light in 1 M acetic acid aqueous solution, as shown in Fig. 4a, on which the modified area (corresponding to the luminescent area in Fig. 4a) showed I_D/I_G values over 1.0 (Fig. S5†). The heterogenous luminescent intensities could be attributed to the spatial heterogeneity of the PICM efficiency caused by the tiny deviation in the laser focus during stage movements (Fig. 4a). Additionally, weak/no luminescent spot corresponds probably to the spots of multiple-layered graphene (details see Fig. S5†). A luminescence spectrum at the modified region is shown in Fig. 4b (excitation: 349 nm). The modified graphene in acetic acid solution emits luminescence around 620 nm (Fig. 4b), which is likely due to fragmentation of π-conjugation in graphene by the PICM. The functional groups-induced localized states in π–π* gap of sp^2 sites in graphene may cause a broad emission band.[29] In addition, functionalized groups, such as C–O, C═O and COOH, could have contribution to the fluorescence.[30] A detailed analysis of the luminescence property is shown in Fig. S6.†

An IR spectrum was taken on the modified area to investigate chemical functionalization on the graphene surface (Fig. 5). Note that graphene's broad IR absorption across the measured frequency range was analytically removed by a 3rd order polynomial fitting to the raw spectrum. From Fig. 5, a number of IR peaks were detected. Those can be assigned to O–H stretching at 3650 cm^{-1} (broad), C–H stretching at 2918 and 2851 cm^{-1}, C═O stretching from ester groups at 1741 cm^{-1}, C═C stretching at 1637 cm^{-1}, C–H bending at

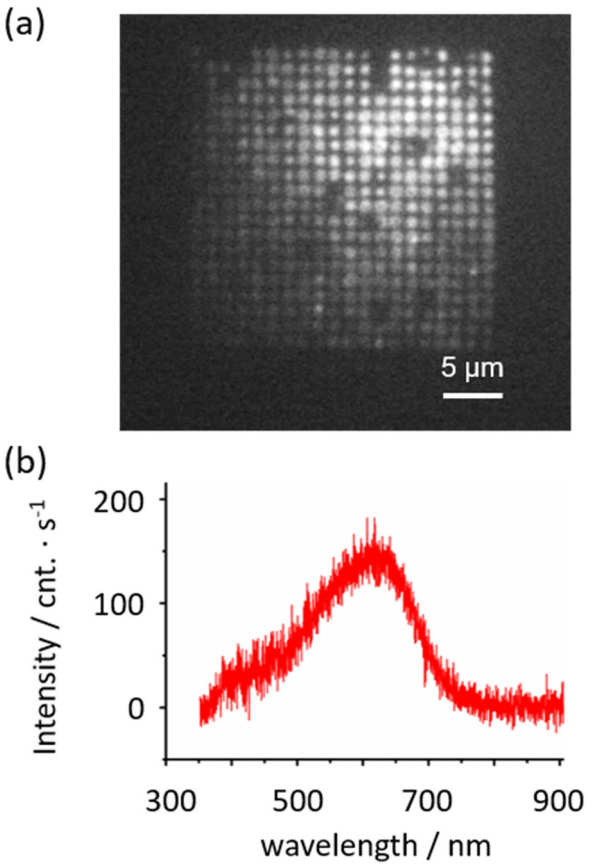

Fig. 4 Luminescence microscopy/spectroscopy after the patterned PICM of a graphene monolayer in acetic acid aqueous solution. (a) Raman/luminescence wide-field image of the modified graphene upon excitation at 488 nm. (b) A luminescence spectrum at the modified area upon excitation at 349 nm.

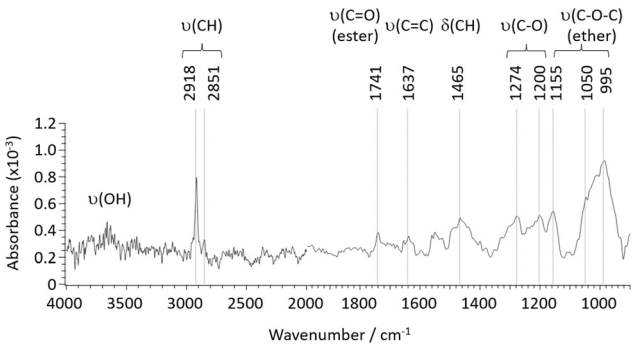

Fig. 5 IR spectrum of a graphene monolayer after the PICM in acetic acid aqueous solution.

Table 1 The reaction rate in H_2O, and aqueous solution (0.1 M) of formic acid, acetic acid, propionic acid, and butyric acid, respectively

Reagents	k (min^{-1})
Water	1.53×10^{-3}
Formic acid	1.32×10^{-3}
Acetic acid (n = 0)	2.98×10^{-1}
Propionic acid (n = 1)	9.42×10^{-2}
Butyric acid (n = 2)	2.92×10^{-2}

1465 cm^{-1}, C–O stretching at 1274 and 1200 cm^{-1}, and C–O–C stretching from ester groups at 1155, 1050 and 995 cm^{-1} (as listed in Table 2). Intense C–H stretching absorption suggests the presence of methyl functional groups on the graphene surface. Also, strong absorption from ether groups (C–O–C stretching) was measured, and, in correspondence with the strong C–H absorption, it is likely that a certain amount of

Table 2 Assignment of IR peaks and expected origins

Wavenumber (cm^{-1})	Assignment	Origin
3650 (broad)	O–H stretching	Hydroxy
2918, 2851	C–H stretching	Methyl, methoxy, acetate
1741	C═O stretching (ester)	Acetate
1637	C═C stretching	Graphene
1465	C–H bending	Methyl, methoxy, acetate
1274, 1200	C–O stretching	Methoxy, acetate
1155, 1050, 995	C–O–C stretching (ether)	Methoxy

methoxy groups exist on the surfaces. Also, from the fingerprint region, C═O and C–O stretching were identified with similar intensities, suggesting the presence of ester and/or carboxylic groups, while the amount of the carboxylic is presumably limited given the weak O–H stretching. Thus, along with the strong C–H absorption, a certain number of acetate group is likely formed on the graphene surface.

From Raman spectroscopy, alteration to the graphene electronic structure *via* PICM is discussed in terms of G-band shape. As presented in Fig. 6a, besides the appearance of D-band, we observed a new peak at lower than 1590 cm^{-1} (denoted as G^-). We found that the newly appeared G-band downshifts with higher PICM degree (Fig. 6a). Since the wavenumber of Raman signal of the G-bands is independent of the laser wavelength (Table S1†), they are likely originated from a first order Raman process. Two peaks in the G-band indicate that two phonon energies are allowed at the Q point (k = 0). It is known that molecular adsorption could induce phonon symmetry breaking, leading to the degeneracy of the transverse optical (TO) and longitudinal optical (LO) phonon modes.[31] In this study, G-band splitting was observed only in SCFAs with an alkyl chain but neither in pure water nor in formic acid aqueous solution (Fig. 2). The downshift of the G-band peak position shows a significant dependence on alkyl chain length, where a larger shift was found on longer alkyl chains (Fig. 6b). The fact that longer alkyl chains have higher electron donating nature further supports the above IR analysis, in which we speculate that alkyl chains are covalently attached to the graphene surface. Indeed, a small peak that could be related to the alkyl group was found at ~2943 cm^{-1} (C–H stretching, ν(CH)[32]) in Raman spectra of highly modified graphene with SCFAs with alkyl chain (see Raman spectra in Fig. S7† and DFT calculation in Fig. S8 and Table S2†).

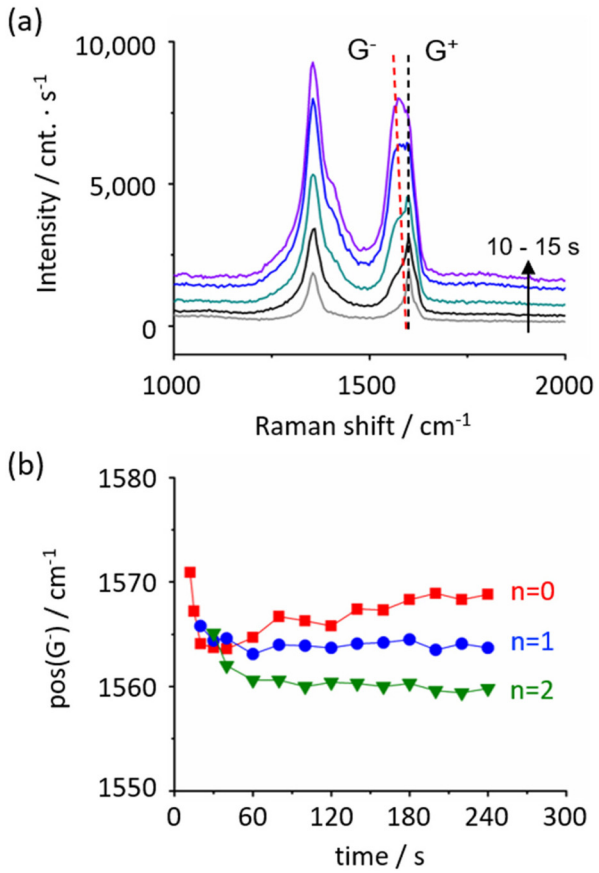

Fig. 6 G-band splitting and downshifting upon the PICM. (a) Raman spectra from 10 to 15 s during PICM on graphene in an aqueous solution of acetic acid (n = 0). The G-band splits into two peaks and one of them downshifts as a function of time. (b) Position of G-peak in an aqueous solution of acetic acid (n = 0) (red), propionic acid (n = 1) (green), and butyric acid (n = 2) (purple) as a function of time, respectively.

Given these results, the possible reaction mechanism is illustrated in Scheme 1. We consider the PICM reaction in the presence of SCFAs with an alkyl chain proceeds in two reaction stages considering the high oxidation efficiency and species of functional groups on graphene. At the initial stage (stage 1), water plays a critical role and oxidative components, such as hydroxyl or carboxyl groups, are introduced on graphene surfaces. This oxidation is initiated by charge separation (*i.e.*, the generation of excitons/hot electrons in graphene) upon light irradiation to graphene, reacting with surrounding water molecules and radicals are stabilized by water solvation.[14,22] Once the oxidative groups are introduced on graphene, these polar sites start to 'capture' holes/electrons migrating on graphene and work as an 'active' reaction site, starting the 2nd stage reaction. In stage 2, the presence of SCFAs with an alkyl chain plays a key role. Due to the radical reaction, high density of methyl, methoxy, and acetate groups seem to be finally introduced on the graphene surface. When the SCFAs with an alkyl chain meet the active site, carboxyl radicals ($CH_3(CH_2)_nCOO^{\bullet}$), as well as alkyl radicals ($CH_3(CH_2)_n^{\bullet}$) that are automatically generated *via* decarboxylation reaction,[33–35] are generated in the solution. These radical species directly attack the pristine graphene surface, functionalizing alkyl and ester groups on the surfaces and/or they attack hydroxyl/carboxyl groups forming ether/ester functionalization. These alkyl groups radicals' reaction is the limiting step in PICM. The two stages properly explain the high PICM efficiency in SCFAs with an alkyl chain. A decrease in reaction rate was indeed observed when increasing the length of the alkyl chains. In stage 2, acetic acid can generate methyl radicals, which are the most reactive because of the primary carbon radical. While propionic and butyric acids can generate ethyl and propyl radicals which are categorized into secondary carbon radicals.

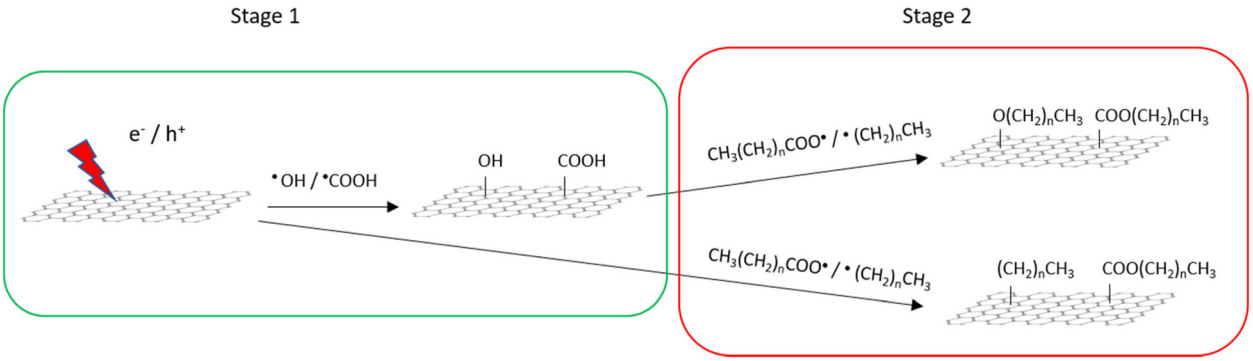

Scheme 1 Possible mechanism of the PICM on graphene in an aqueous solution of SCFAs with an alkyl chain.

Generally, the reaction rate of molecules with smaller molecular weights is faster than those with larger molecular weights.

Conclusions

We have introduced dense functionalization on graphene by SCFAs with an alkyl chain in an aqueous solution using a simple liquid-phase PICM method. By this method, it is easy to wash out the aqueous solution after reaction and can be used to employ modified graphene as a material. We found that, compared to the PICM in water, SCFAs with an alkyl chain drastically enhance the PICM efficiency, most likely due to radical reactions. It takes only several seconds to reach $I_D/I_G \approx 1$.

IR and Raman spectroscopy reveal high-density modification of graphene with methyl, methoxy, and acetate groups. A greater downshift of the G-band in Raman spectra was observed upon PICM with longer alkyl chains, suggesting that the charge doping effect can be controlled by the alkyl chain length of the SCFAs. These results suggest that, together with laser-assisted radical reactions, sub-micrometre scaled, site-elective bandgap engineering can be applied to graphene surfaces, opening a venue for micro-scale graphene device applications.

Author contributions

G.F. investigated the experiment and wrote the original draft. T.I. and H.W. contributed to Raman measurements. N.S. performed the DFT calculation and data analysis. F.T. and M.W. reviewed and edited the manuscript. S.T., Y.F. and K.H. discussed the results and co-wrote the manuscript. Y.F. performed the IR measurement and data analysis. H.U. supervised the experiment and co-wrote the manuscript. All the authors proofread and approved the final manuscript for submission.

Conflicts of interest

There are no conflicts to declare.

Acknowledgements

This work was supported by JSPS Kakenhi (Grants # 19KK0136, 20K21200, 20K05413, 21H04634, 21K18871, 22H00328, 21H01740, 22K20524), Research Foundation of Flanders (FWO) research grant (G081916N) and KU Leuven – Internal Funds. T. I. thanks to JST PRESTO (JPMJPR2104). G. F. and H. W. greatly thanks to the financial support of the China Scholarship Council (CSC) and the DX fellowship of Hokkaido University, respectively. We thank the Open Facility, Global Facility Center, Creative Research Institution, Hokkaido University for allowing us to use SEM, STEM and XRD. This collaborative work was greatly supported by JSPS Core-to-Core Program, A. Advanced Research Networks.

References

1 Z. Sun, C. L. Pint, D. C. Marcano, C. Zhang, J. Yao, G. Ruan, Z. Yan, Y. Zhu, R. H. Hauge and J. M. Tour, *Nat. Commun.*, 2011, **2**, 559.
2 A. N. Grigorenko, M. Polini and K. S. Novoselov, *Nat. Photonics*, 2012, **6**, 749–758.
3 Q. Xiang, J. Yu and M. Jaroniec, *Chem. Soc. Rev.*, 2012, **41**, 782–796.
4 G. Reina, J. M. Gonzalez-Dominguez, A. Criado, E. Vazquez, A. Bianco and M. Prato, *Chem. Soc. Rev.*, 2017, **46**, 4400–4416.
5 R. Ye and J. M. Tour, *ACS Nano*, 2019, **13**, 10872–10878.
6 G. Zhao, X. Li, M. Huang, Z. Zhen, Y. Zhong, Q. Chen, X. Zhao, Y. He, R. Hu, T. Yang, R. Zhang, C. Li, J. Kong, J. B. Xu, R. S. Ruoff and H. Zhu, *Chem. Soc. Rev.*, 2017, **46**, 4417–4449.
7 L. Lin, H. Peng and Z. Liu, *Nat. Mater.*, 2019, **18**, 520–524.
8 B. Luo and L. Zhi, *Energy Environ. Sci.*, 2015, **8**, 456–477.
9 Z. Sun, S. Fang and Y. H. Hu, *Chem. Rev.*, 2020, **120**, 10336–10453.
10 X. Xu, C. Liu, Z. Sun, T. Cao, Z. Zhang, E. Wang, Z. Liu and K. Liu, *Chem. Soc. Rev.*, 2018, **47**, 3059–3099.
11 Y. Chen, B. Zhang, G. Liu, X. Zhuang and E. T. Kang, *Chem. Soc. Rev.*, 2012, **41**, 4688–4707.

12 Y. Xia, L. Sun, S. Eyley, B. Daelemans, W. Thielemans, J. Seibel and S. De Feyter, *Adv. Sci.*, 2022, **9**, 2105017.
13 M. C. Rodríguez González, A. Leonhardt, H. Stadler, S. Eyley, W. Thielemans, S. De Gendt, K. S. Mali and S. De Feyter, *ACS Nano*, 2021, **15**, 10618–10627.
14 S. Toyouchi, M. Wolf, G. Feng, Y. Fujita, B. Fortuni, T. Inose, K. Hirai, S. De Feyter and H. Uji-i, *J. Phys. Chem. Lett.*, 2022, **13**, 3796–3803.
15 H. Hu, C. C. K. Allan, J. Li, Y. Kong, X. Wang, J. H. Xin and H. Hu, *Nano Res.*, 2014, **7**, 418–433.
16 J. T. Robinson, J. S. Burgess, C. E. Junkermeier, S. C. Badescu, T. L. Reinecke, F. K. Perkins, M. K. Zalalutdniov, J. W. Baldwin, J. C. Culbertson, P. E. Sheehan and E. S. Snow, *Nano Lett.*, 2010, **10**, 3001–3005.
17 J. Greenwood, T. H. Phan, Y. Fujita, Z. Li, O. Ivasenko, W. Vanderlinden, H. Van Gorp, W. Frederickx, G. Lu, K. Tahara, Y. Tobe, H. Uji-i, S. F. L. Mertens and S. De Feyter, *ACS Nano*, 2015, **9**, 5520–5535.
18 L. Bao, B. Zhao, B. Yang, M. Halik, F. Hauke and A. Hirsch, *Adv. Mater.*, 2021, **33**, 2101653.
19 Y. Zhou and K. P. Loh, *Adv. Mater.*, 2010, **22**, 3615–3620.
20 W. Zhang, Y. Lei, F. Ming, Q. Jiang, P. M. F. J. Costa and H. N. Alshareef, *Adv. Energy Mater.*, 2018, **8**, 1801840.
21 H. Liu, S. Ryu, Z. Chen, M. L. Steigerwald, C. Nuckolls and L. E. Brus, *J. Am. Chem. Soc.*, 2009, **131**, 17099–17101.
22 N. Mitoma, R. Nouchi and K. Tanigaki, *J. Phys. Chem. C*, 2013, **117**, 1453–1456.
23 K. Xia, W. Y. Chiang, C. J. Lockhart de la Rosa, Y. Fujita, S. Toyouchi, H. Yuan, J. Su, H. Masuhara, S. De Gendt, S. De Feyter, J. Hofkens and H. Uji-i, *Nanoscale*, 2020, **12**, 11063–11069.
24 K. F. Edelthalhammer, D. Dasler, L. Jurkiewicz, T. Nagel, S. Al-Fogra, F. Hauke and A. Hirsch, *Angew. Chem., Int. Ed.*, 2020, **59**, 23329–23334.
25 P. Venezuela, M. Lazzeri and F. Mauri, *Phys. Rev. B*, 2011, **84**, 035433.
26 T. T. You, N. Yang, Y. Q. Shu and P. G. Yin, *J. Raman Spectrosc.*, 2019, **50**, 1510–1518.
27 A. Eckmann, A. Felten, I. Verzhbitskiy, R. Davey and C. Casiraghi, *Phys. Rev. B*, 2013, **88**, 035426.
28 C. F. Chen, C. H. Park, B. W. Boudouris, J. Horng, B. Geng, C. Girit, A. Zettl, M. F. Crommie, R. A. Segalman, S. G. Louie and F. Wang, *Nature*, 2011, **471**, 617–620.
29 C. T. Chien, S. S. Li, W. J. Lai, Y. C. Yeh, H. A. Chen, I. S. Chen, L. C. Chen, K. H. Chen, T. Nemoto, S. Isoda, M. Chen, T. Fujita, G. Eda, H. Yamaguchi, M. Chhowalla and C. W. Chen, *Angew. Chem., Int. Ed.*, 2012, **51**, 6662–6666.
30 J. Shang, L. Ma, J. Li, W. Ai, T. Yu and G. G. Gurzadyan, *Sci. Rep.*, 2012, **2**, 792.
31 X. Dong, Y. Shi, Y. Zhao, D. Chen, J. Ye, Y. Yao, F. Gao, Z. Ni, T. Yu, Z. Shen, Y. Huang, P. Chen and L. J. Li, *Phys. Rev. Lett.*, 2009, **102**, 135501.
32 G. Socrates, *Infrared and Raman Characteristic Group Frequencies: Tables and Charts*, J. Wiley and Sons, Chichester, 3rd edn, 2001, p. 12.
33 Y. B. Lim, Y. Tan and B. J. Turpin, *Atmos. Chem. Phys.*, 2013, **13**, 8651–8667.
34 A. Bhattacherjee, M. Sneha, L. Lewis-Borrell, O. Tau, I. P. Clark and A. J. Orr-Ewing, *Nat. Commun.*, 2019, **10**, 5152.
35 Y. Yoshimi, T. Itou and M. Hatanaka, *Chem. Commun.*, 2007, 5244–5246.